

# Design Optimization of Pyramid-Shaped Transmission System for Multi-Arm Concentric-Tube Robots

Chao Zhang<sup>1</sup>, Guangdu Cen<sup>1</sup>, Xing Yang<sup>1</sup>, Xinhai Xu<sup>1</sup>, Max Q.-H. Meng<sup>2</sup>, Shuang Song<sup>1,\*</sup>, Jiaole Wang<sup>1,\*</sup>

**Abstract**—Pyramid-shaped transmission system of multi-arm concentric-tube robots (CTR) possesses advantages of convenient arrangement and collision avoidance of its actuation units. However, design optimization of such transmission system has not been systematically studied. This paper presents an optimal design framework of pyramid-shaped transmission system for multi-arm CTR. Each arm of the CTR consists of several telescoped tubes, and the tube is made by a pre-curved super-elastic NiTi tube bonded to a straight stainless steel (SS) tube which transmits torsion and translation to the distal NiTi tube. The SS tubes inclinedly stretch into a bending unit and exit parallelly. Geometric constraints of the transmission system, including the relations of tube diameters, the shape and length of SS tube, and the collision of actuation units, are first introduced. Secondly, deformation constraints considering the bending and torsional twisting of SS tubes are derived. Lastly, the design problem has been formulated as a constrained nonlinear multi-objective optimization problem that minimizes both the twist of the tube and the size of the whole system. Based on the proposed framework, we demonstrate the design workflows of the pyramid-shaped transmission system for two sets of NiTi manipulators. Numerical simulations and real-world experiments have been conducted to validate the efficacy of the proposed modeling and optimization methods.

**Index Terms**—Design optimization, multi-arm concentric-tube robot, pyramid-shaped transmission system.

## I. INTRODUCTION

**C**ONCENTRIC-TUBE robots (CTR) are ideally suitable for medical diagnosis and minimally-invasive surgery (MIS) because of their compact profile (diameter  $\approx 1 \sim 3$  mm) [1]–[4]. A typical single-arm CTR is comprised of several telescoped pre-curved super-elastic NiTi tubes. Each tube can be translated and rotated relative to each other by an actuation module connected at its proximal end. Kinematic input of the actuation modules and the elastic interactions between the tubes generate a final robot shape [5].

Compared with single-arm CTR, although multi-arm CTR increases the overall dimensions of system, it allows for collaboration of multiple manipulators to execute complex surgical tasks such as tissue excision and suturing. In this context, Burgner-Kahrs *et al.* [6] proposed a bi-manual CTR for transnasal surgery. Its two actuation units were arranged in parallel and the center distance between two arms was 35

<sup>1</sup>Chao Zhang, Guangdu Cen, Xing Yang, Xinhai Xu, Shuang Song and Jiaole Wang are with School of Mechanical Engineering and Automation, Harbin Institute of Technology (Shenzhen), Shenzhen, China, 518055.

<sup>2</sup>Max Q.-H. Meng is with the Department of Electronic Engineering of the Southern University of Science and Technology in Shenzhen, China, on leave from the the Department of Electronic Engineering , the Chinese University of Hong Kong (CUHK), Hong Kong, and also with the Shenzhen Research Institute of the CUHK in Shenzhen, China.

\*Corresponding authors: J. Wang [wangjiaole@hit.edu.cn](mailto:wangjiaole@hit.edu.cn) and S. Song [songshuang@hit.edu.cn](mailto:songshuang@hit.edu.cn)

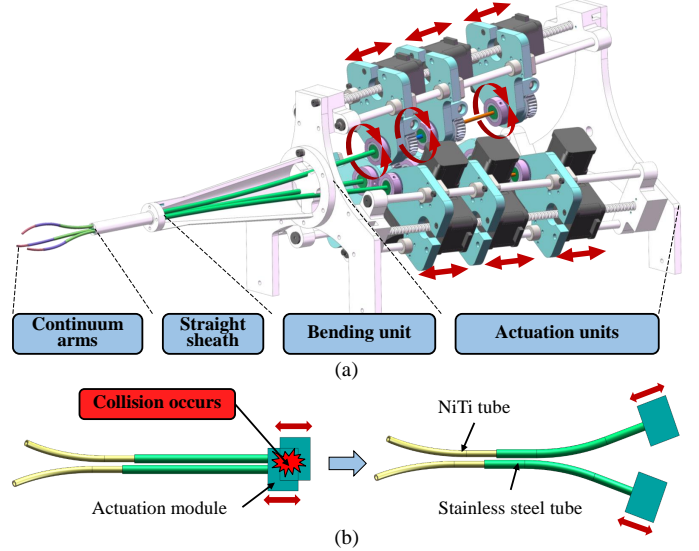


Fig. 1. (a) is the proposed multi-arm CTR with pyramid-shaped transmission system. It mainly consists of actuation units, a bending unit, a straight sheath and continuum robotic arms. The actuation units and the arms are arranged symmetrically in space. (b) shows two types of transmission system for multi-arm CTR. The left one is the parallel configuration where the actuation units are arranged in parallel, and the right one is the Y- or pyramid-shaped configuration in which the actuation units are arranged at an angle.

mm. Richard *et al.* [7] and Fox *et al.* [8] respectively developed a dual-arm CTR system clinically used for transurethral procedures and neurosurgery, their actuation units were also arranged in parallel and the NiTi manipulators were constricted through an endoscope. In [9] and [10], similar parallel-arranged transmission systems were adopted in their multi-arm CTR designed for single-port surgery. In summary, for the multi-arm CTR used in single-port MIS, the center distance between arms needs to be reduced to better meet surgical requirements. Consequently, as depicted in Fig. 1 (b), the parallel arranged actuation units of these multi-arm CTR are easy to interfere and collide, and it is difficult to design and assemble the actuation units due to the strictly limited space.

To alleviate this problem, Y- and pyramid-shaped transmission systems for multi-arm CTR have been proposed. As shown in Fig. 1 (b), their main characteristics are that the tubes are bent to reduce the center distance between arms and facilitate the collision-free motion of the actuation units. Azimian *et al.* [11] developed a dual-arm CTR for the neuroendoscopic. The straight segments of tubes were arranged at an angle and then collected by a trocar, which formed a Y-shaped configuration. In fact, the Y-shaped transmission system can be regarded as a two-dimensional case of the pyramid-shaped

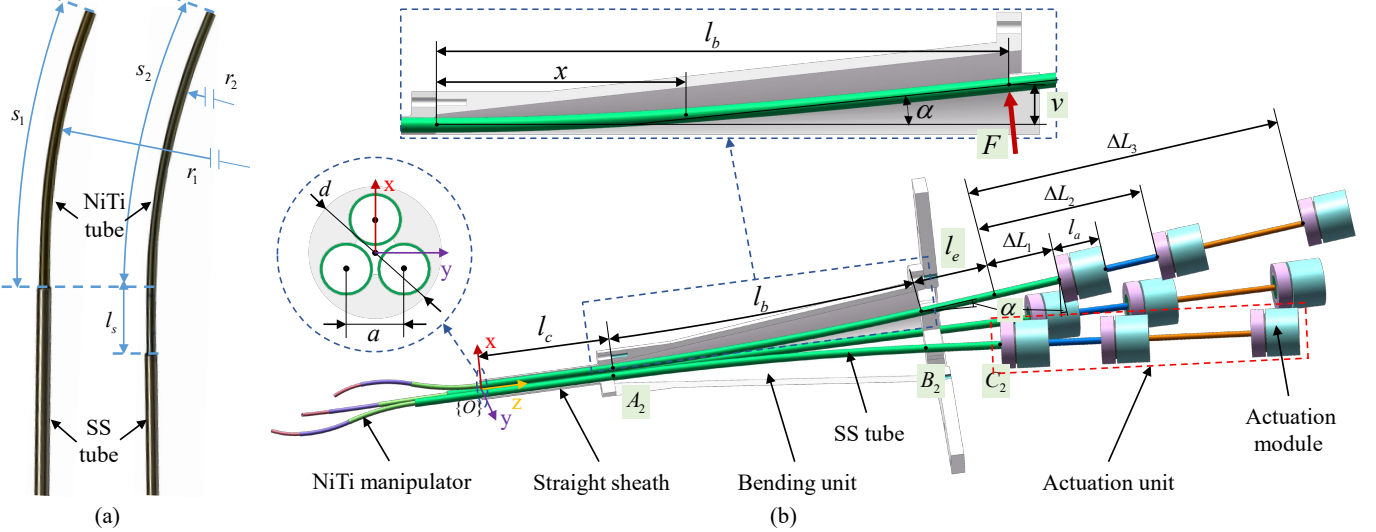


Fig. 2. (a) Two “SS + NiTi” tubes. Each pre-curved NiTi tube is bonded to the corresponding straight SS tube via cyanoacrylate adhesive (Loctite 480). Diagram of the pyramid-shaped transmission system of a multi-arm CTR using “SS + NiTi” tubes. (b) The transmission system mainly consists of the actuation modules in the actuation units, the bending unit, the straight sheath and the SS tube segment of each “SS + NiTi” tube.

ones. In [12], Mitros *et al.* presented a multi-arm CTR system for the optic nerve sheath fenestration. It adopted a quasi pyramid-shaped transmission system so that its actuation units could be placed readily. Bruns *et al.* [13] developed a modular, pyramid-shaped, and multi-arm CTR which was applied to transnasal surgery for orbital tumors. Besides, to deliver multiple arms within a steerable sheath for single-port MIS, eccentric-tube robots have been presented with small center distances between its eccentrically arranged continuum arms [14]–[18], and the pyramid-shaped transmission system is an ideal transmission scheme for them.

Although multi-arm CTR with pyramid-shaped transmission system possess many advantages, such configuration will increase tube lengths resulting in larger torsional twisting of NiTi tubes. To tackle this problem, stainless steel (SS) tubes that have greater stiffness than NiTi tubes are used to transmit motions [13], [19], as shown in Fig. 2 (a). This method was also successfully adopted in [12], [20], [21] to reduce the torsional deformation and build-up strain energy of NiTi tubes which can cause elastic instability (sudden snapping of tubes to reach a configuration with lower elastic energy).

At present, literatures on the design optimization of CTR mainly focus on NiTi manipulators [22]–[24], and little of them is about the optimal design of the transmission system, let alone the pyramid-shaped transmission system for multi-arm CTR. Nevertheless, how to design a suitable pyramid-shaped transmission system is an inevitable problem in the design of a multi-arm CTR. If the transmission system is not optimally designed, the empirically designed result may lead to inappropriate designed parameters, which could fail to meet the design requirements and even cause snapping of NiTi arms.

In this paper, an optimal design framework of the pyramid-shaped transmission system for multi-arm CTR is proposed. Given design parameters of NiTi manipulators according to specific MIS tasks, we can establish the geometric and deformation constraints of the transmission system. Then, the

design problem can be formulated as a constrained nonlinear multi-objective optimization problem which minimizes both the twisting of tubes and the size of whole system. Solving the problem, the optimal design parameters of the transmission system can be determined.

The contributions of this paper are: (1) an optimal design framework of the pyramid-shaped transmission system for multi-arm CTR is proposed for the first time to our best knowledge, (2) a multi-arm CTR with optimal transmission system and the accompanying code have been presented.

## II. PROBLEM DESCRIPTION

### A. Pyramid-Shaped Transmission System

As shown in Fig. 1 (a), a multi-arm CTR with pyramid-shaped transmission system is proposed in this paper. It is mainly composed of several actuation units, a bending unit, a straight sheath and multiple continuum arms. To alleviate the torsional twisting of NiTi tubes, SS tubes that have greater torsional stiffness than NiTi tubes are used to span much of the length from their actuation modules to the base of NiTi arms. The pre-curved NiTi tube is glued to a straight SS tube via cyanoacrylate adhesive (Loctite 480), which forms a “SS + NiTi” tube as illustrated in Fig. 2 (a). Each continuum arm consists of several telescoped “SS + NiTi” tubes, the proximal end of each SS tube is attached to an actuation module in the corresponding actuation unit. The straight SS tubes stretch into the bending unit, and the bending unit bends these tubes and makes them stretch out parallelly. Then, the straight sheath collects these SS tubes together, thus these SS tubes and their actuation units are constrained into a pyramid-shaped configuration. The actuation module provides translation and rotation to its corresponding SS tube, and then the SS tube transmits motions to the distal NiTi tube. Finally, the kinematic input of actuation modules and the elastic interactions between NiTi tubes generate the final shapes of the continuum arms.

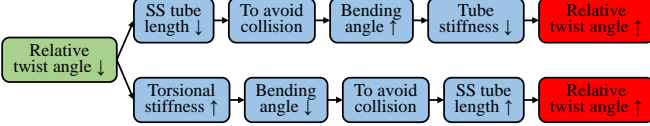


Fig. 3. The trade-off of design parameters in the design of pyramid-shaped transmission system by minimizing the maximum relative twist angle of a SS tube between its proximal and distal end.

### B. Design Optimization Problem

As shown in Fig. 2 (b), the pyramid-shaped transmission system for the CTR mainly contains the actuation units, the bending unit, the straight sheath and the SS tubes in all the “SS + NiTi” tubes. Because this paper focuses on the transmission system design, it is assumed that the parameters of NiTi manipulators have been given according to specific MIS tasks. Therefore, the transmission system design is mainly to determine its design parameters properly, such as the SS tube diameters, the tube bending angle and so on.

However, these design parameters are subject to many constraints, and we need to trade them off for the optimal values. For example, see Fig. 3, if we require a minimum relative twist angle between the proximal and distal end of a SS tube, we should reduce the tube length and increase the torsional stiffness, which means a shorter and thicker SS tube. However, it will decrease the maximum bending angle of the SS tube because of the elastic strain limit, which in turn needs to increase the tube length to avoid collision of actuation units. Therefore, a design optimization problem can be formulated here by optimizing the relative twist angle of the SS tube and considering the design constraints.

To formulate the design optimization problem, we first define the optimization variable as

$$\mathbf{x} = [OD_{S_1}, OD_{S_2}, \dots, OD_{S_m}, l_b, \alpha, l_e, \beta_1, \beta_2, \dots, \beta_{n-1}]^T \quad (1)$$

which is an  $(m + n + 2)$ -dimensional vector for a CTR with  $n$  identical arms and each arm with  $m$  telescoped tubes, and the definitions of every element in  $\mathbf{x}$  will be introduced later.

Depending on the requirements of transmission system for a multi-arm CTR, there are two optimization objectives that are of main concerns. One is to minimize the maximum relative twist angle of the SS tube  $\zeta_{i_{max}}$  to obtain a smaller kinematic input error from the actuation module to the base of the NiTi tube, and the objective function can be written as

$$F_1(\mathbf{x}) = \zeta_{i_{max}}. \quad (2)$$

The other is to minimize the SS tube length  $L_i$  to make the transmission system more compact. As  $l_c$  and  $\Delta L_i$  are pre-defined for each SS tube, their lengths can be represented by

$$F_2(\mathbf{x}) = l_b + l_e. \quad (3)$$

## III. DESIGN CONSTRAINTS

### A. Geometric Constraints

1) *Diameter Relations of Tubes:* As shown in Fig. 4, for an  $n$ -armed CTR with  $m$  “SS + NiTi” tubes in each arm, tube diameters should be properly determined to meet the assembly constraints. For the NiTi tubes, their parameters are

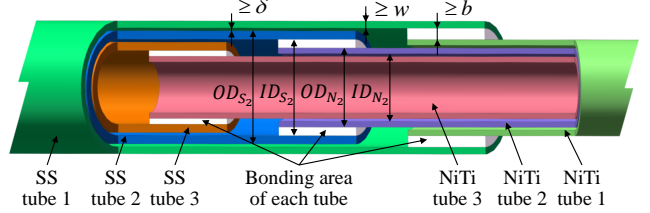


Fig. 4. Partial section view of a continuum arm with three telescoped “SS + NiTi” tubes.

pre-defined,  $OD_{N_i}$  and  $ID_{N_i}$  respectively denote the outer and inner tube diameters, and subscript indices  $i = 1, \dots, m$  refer to individual tubes with tube 1 being outermost and tube  $m$  being innermost. For the SS tubes,  $OD_{S_i}$  and  $ID_{S_i}$  denote the outer and inner tube diameters, and they should satisfy

$$\begin{cases} ID_{S_i} \geq OD_{N_i} + 2b \\ OD_{S_i} \geq ID_{S_i} + 2w \end{cases} \quad (4)$$

in which  $b$  is the minimum allowable bonding thickness, and  $w$  is the minimum wall thickness of the SS tube.

From the perspective of proper assembly clearance, the diameters of adjacent SS tubes should meet

$$OD_{S_i} = ID_{S_{i-1}} - 2\delta \quad (5)$$

where  $\delta$  denotes the maximum assembly clearance between two adjacent SS tubes and  $i = 2, \dots, m$ .

As shown in Fig. 2 (b), the center distance  $a$  between adjacent robotic arms and the circumcircle diameter  $d$  of all arms measured at the end of the straight sheath are pre-defined according to the size requirements of incision or natural orifice in single-port MIS, and they need to satisfy

$$\begin{cases} OD_{S_1} \leq a \\ OD_{S_1} + a/\sin(\pi/n) \leq d \end{cases} \quad (6)$$

From (4), (5) and (6), the diameter relations of these  $m$  “SS + NiTi” tubes in each robotic arm can be formulated as

$$\mathbf{A} [OD_{S_1}, \dots, OD_{S_m}]^T \leq \mathbf{b} \quad (7)$$

which is a linear inequality constraint of  $OD_{S_i}$ ,  $\mathbf{A} \in \mathbb{R}^{2m \times m}$  and  $\mathbf{b} \in \mathbb{R}^{2m \times 1}$  are coefficient matrices.

2) *Shape and length of SS Tubes:* The formation of the pyramid-shaped transmission system is mainly due to the constraints of the bending unit and straight sheath. As shown in the top of Fig. 2 (b), the bending segment of a SS tube can be regarded as a beam, which has a build-in support at the left and is subjected to an applied force  $F$  at the right.  $v(x)$  and  $\alpha(x)$  are the deflection and tangent angle of the SS tube’s central axis relative to the straight  $x$  axis, respectively.

The deflection can be characterized by Euler–Bernoulli beam theory [25] because of the small bending angle, and the second order derivative of the tube’s central axis deflection is approximate to

$$\ddot{v}(x) = \frac{F}{EI} (l_b - x) \quad (8)$$

in which  $E$  is the elastic modulus of SS material,  $I$  is the SS tube’s cross-sectional moment of inertia, and  $l_b$  is the arc length of the SS tube bending segment.

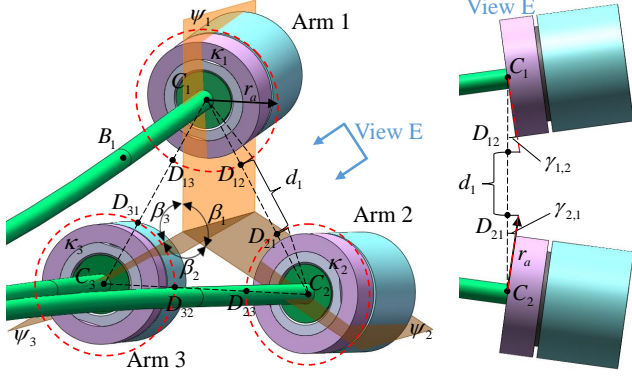


Fig. 5. The pyramid-shaped transmission system when the first actuation module of each actuation unit reaches its forward limiting position. Only actuation module 1 and SS tube 1 in each arm are considered. View E is perpendicular to the plane determined by points  $B_1$ ,  $C_1$  and  $C_2$ .

By integrating (8) and including boundary conditions  $\dot{v}(0) = 0$ ,  $v(0) = 0$ , yielding

$$\dot{v}(x) = \tan \alpha(x) = \frac{F}{2EI} (2l_b x - x^2) \quad (9)$$

$$v(x) = \frac{F}{2EI} \left( l_b x^2 - \frac{x^3}{3} \right). \quad (10)$$

At the right end of the bending segment, we can get their maximum values as

$$\alpha = \arctan \left( \frac{Fl_b^2}{2EI} \right) \quad (11)$$

$$v = \frac{Fl_b^3}{3EI} = \frac{2}{3} l_b \tan \alpha \quad (12)$$

in which  $\alpha$  and  $v$  refer to  $\alpha(l_b)$  and  $v(l_b)$  for simplicity, and  $\alpha$  also stands for the bending angle of the bending unit.

For the length of each SS tube, when the distal end of the tube is aligned with the output end of the straight sheath, it can be expressed as

$$L_i = l_c + l_b + l_e + \Delta L_i \quad (13)$$

in which  $l_c$  is the length of the straight sheath,  $\Delta L_i$  is the distance from the proximal end of  $i$ -th SS tube to the forward limiting position of the first actuation module, and  $l_e$  is the length of the tube transition segment from the forward limiting position of first actuation module to the starting point of the tube bending segment. Furthermore,  $l_e$  need to be greater than a minimum length  $l_{e_{min}}$  for the assembly requirements of the bending unit, yielding

$$l_e \geq l_{e_{min}}. \quad (14)$$

3) *Collision Avoidance of Actuation Units:* As illustrated in Fig. 5, the minimum distance between every two adjacent actuation units  $d_j$  ( $j = 1, \dots, n$ ) needs to be calculated to avoid collision between them. Obviously,  $d_j$  occurs when the first actuation module in each actuation unit reaches the forward limiting position.

The symmetry plane of each arm  $\psi_j$  bisects the SS tube, and the angle between adjacent symmetry planes is  $\beta_j$  which indicates the spatial distribution angle of actuation units. We

first establish a coordinate frame  $\{O\}$  at the end of the straight sheath. Then, the spatial position of point  $A_j$ ,  $B_j$  and  $C_j$  on the SS tube of  $j$ -th arm can be deduced relative to frame  $\{O\}$ . For the  $j$ -th arm,  $\overrightarrow{B_j C_j}$  of the SS tube is perpendicular to the plane  $\kappa_j$  of the corresponding first actuation module, so the normal vector of the plane  $\kappa_j$  is

$$\mathbf{n}_j = \overrightarrow{C_j B_j} / |\overrightarrow{C_j B_j}|. \quad (15)$$

Connecting adjacent points  $C_j$  and  $C_{j+1}$ , the line segment  $\overrightarrow{C_j C_{j+1}}$  intersects the plane  $\kappa_j$  and  $\kappa_{j+1}$ , and the included angle between the line and the planes can be expressed as

$$\begin{cases} \gamma_{j,j+1} = \arcsin \left( \mathbf{n}_j^\top \overrightarrow{C_j C_{j+1}} / |\overrightarrow{C_j C_{j+1}}| \right) \\ \gamma_{j+1,j} = \arcsin \left( \mathbf{n}_{j+1}^\top \overrightarrow{C_{j+1} C_j} / |\overrightarrow{C_{j+1} C_j}| \right) \end{cases} \quad (16)$$

in which  $\gamma_{j,j+1} \in (0, \pi/2)$  denotes the angle between the plane  $\kappa_j$  and vector  $\overrightarrow{C_j C_{j+1}}$ , and  $\gamma_{j+1,j} \in (0, \pi/2)$  the angle between plane  $\kappa_{j+1}$  and  $\overrightarrow{C_{j+1} C_j}$ .

To cope with different design of the actuation modules, without loss of generality, we draw a circle with radius  $r_a$  on the plane  $\kappa_j$  with point  $C_j$  being the center, which serves as the collision hazard region for the actuation module. Therefore, we can get the length of line segments  $\overrightarrow{C_j D_{j,j+1}}$  and  $\overrightarrow{C_{j+1} D_{j+1,j}}$  by projecting the radius  $r_a$  onto the line  $\overrightarrow{C_j C_{j+1}}$ . Then, the minimum distance between two adjacent actuation units  $d_j$  ( $j = 1, \dots, n - 1$ ) can be obtained as

$$d_j = |\overrightarrow{C_j C_{j+1}}| - r_a (\cos \gamma_{j,j+1} - \cos \gamma_{j+1,j}). \quad (17)$$

For the case from arm  $n$  to arm 1, we can use the same modeling methods in (16) and (17) with minor modifications. Finally, the constraint for collision avoidance of actuation units can be established as

$$d_j \geq 0. \quad (18)$$

## B. Deformation Constraints

1) *Elastic Strain Limit of Bending:* For the pyramid-shaped transmission system, the initially straight SS tubes are bent to states with curvature  $u$ , which will generate the bending strain in SS tubes as

$$\epsilon = ru \quad (19)$$

in which  $r$  denotes the radius of SS tube.

According to the constitutive law [25] and (8), the curvature  $u$  along the SS tube bending segment can be written as

$$u(x) = \ddot{v}(x). \quad (20)$$

As (20) is a monotonically decreasing function, so we can get the maximum curvature at  $x = 0$ , as

$$u_{max} = \frac{F}{EI} l_b = 2 \tan \alpha / l_b. \quad (21)$$

Thus, the maximum strain occurs when (19) is evaluated at the outer diameter of the outermost SS tube with maximum curvature, that is

$$\epsilon_{max} = (OD_{S_1} \tan \alpha) / l_b. \quad (22)$$

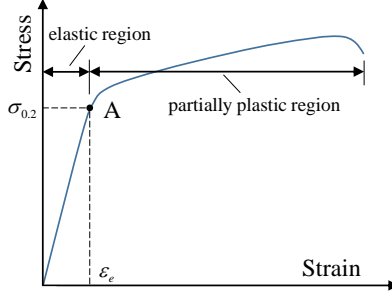


Fig. 6. Typical stress-strain diagram of stainless steel which do not have sharply defined yield point. Point A represents the elastic limit (yield strength) of the material. Beyond point A is called partially plastic region in which the material deforms permanently.

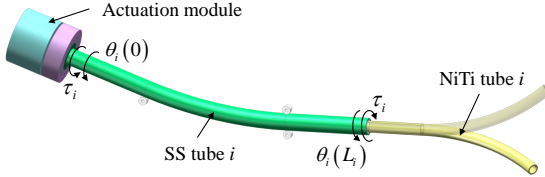


Fig. 7. Torsional twisting of the SS tube segment of an ‘‘SS + NiTi’’ tube. The actuation module drives the SS tube to rotate by  $\theta_i(0)$ , but the actual rotation angle at the distal end of the SS tube  $\theta_i(L_i) \neq \theta_i(0)$  because of its torsional twisting.

As shown in Fig. 6, if  $\epsilon_{max}$  exceeds the elastic deformation limit of the SS material [26], the tube will be plastically deformed and its mechanical properties will change. Thus,  $\epsilon_{max}$  should be limited within the elastic strain limit  $\epsilon_e$  to prevent the plastic deformation of SS tubes, yielding

$$\epsilon_{max} \leq \epsilon_e \quad (23)$$

**2) Torsional Twisting of SS Tubes:** For the ‘‘SS + NiTi’’ tube, the SS tube is used to transmit motions from the actuation module to the NiTi tube. As depicted in Fig. 7, although the SS tube has greater stiffness than the NiTi tube, the torsional twisting between the proximal and distal end of the SS tube can not be ignored if its length is excessive. And such twisting can be characterized by the relative twist angle

$$\zeta_i = \theta_i(0) - \theta_i(L_i) \quad (24)$$

where  $\theta_i(0)$  is the  $i$ -th SS tube’s rotation angle at its proximal end, which is the kinematic input, and  $\theta_i(L_i)$  is the rotation angle at the distal end of the SS tube. Obviously,  $\zeta_i$  will introduce error into the kinematic input for the NiTi tube.

Here, we assume that friction between SS tubes as well as that between the outermost SS tube and the bending unit are neglected, as they are much smaller than the generated torque of the distal NiTi manipulators. Then, the relative twist angle  $\zeta_i$  can be calculated as

$$\zeta_i = \int_{L_i} \frac{\tau_i}{GJ_i} ds \quad (25)$$

in which  $G$  is the sheer modulus of SS material and

$$J_i = \pi (OD_{S_i}^4 - ID_{S_i}^4) / 32 \quad (26)$$

is the SS tube cross-sectional polar moment of inertia,  $\tau_i$  is the torque applied to the SS tube by the actuation module. On

the assumption of friction free between SS tubes,  $\tau_i$  equals to the reverse torque generated by the elastic interaction of NiTi manipulator, and it can be measured using torque sensors [27] or derived by the torsionally compliant model of NiTi manipulator [5], [28].

The maximum relative twist angle of the  $i$ -th SS tube occurs when  $\tau_i$  takes its maximum value, yielding

$$\zeta_{i_{max}} = \frac{32\tau_{i_{max}} L_i}{\pi G (OD_{S_i}^4 - ID_{S_i}^4)}. \quad (27)$$

We demand that  $\zeta_{i_{max}}$  of each SS tube is equal so as to reduce the average kinematic input error for the NiTi tubes. Meanwhile,  $\zeta_{i_{max}}$  should not exceed a maximum allowable value  $\zeta_{max}^d$  defined by designers according to the transmission accuracy requirement, yielding

$$\zeta_{1_{max}} = \dots = \zeta_{m_{max}} \leq \zeta_{max}^d. \quad (28)$$

#### IV. OPTIMIZATION METHOD

##### A. Optimization Problem Formulation

In Section II, we have presented the two optimization objectives  $F_1(\mathbf{x}) = \zeta_{i_{max}}$  and  $F_2(\mathbf{x}) = (l_b + l_e)$ . The design constraints of the transmission system have been also modeled in Section III. However, it is difficult for the two objectives to obtain optimal values at the same time, and the trade-offs between them need to be revealed so as to determine the final optimal design results.

Here, multi-objective optimization method is adopted to find out the possible Pareto optimal solutions, and the optimization problem can be formulated as

$$\mathbf{x}^* = \arg \min_{\mathbf{x}} [F_1(\mathbf{x}), F_2(\mathbf{x})] \quad (29)$$

$$\begin{aligned} & \mathbf{A} [OD_{S_1}, \dots, OD_{S_m}]^\top \leq \mathbf{b} \\ & l_e \geq l_{e_{min}} \\ & s.t. \quad d_i \geq 0, \quad i = 1, 2, \dots, n \\ & \epsilon_{max} \leq \epsilon_e \\ & \zeta_{1_{max}} = \dots = \zeta_{m_{max}} \leq \zeta_{max}^d \end{aligned} \quad (30)$$

It is a constrained nonlinear multi-objective optimization problem, and  $[F_1(\mathbf{x}), F_2(\mathbf{x})]$  is a vector of objectives, if any components in it is competing, there is no unique solution to this problem. Instead, the noninferior solution is used to characterize the trade-offs of objectives, and a noninferior solution is one in which an improvement in one objective requires the degradation of another. Solving the above optimization problem, a Pareto front can be gotten as illustrated in Fig. 8, which is the set of noninferior solutions.

In Fig. 8,  $A$  and  $B$  are the points where  $F_1(\mathbf{x})$  and  $F_2(\mathbf{x})$  obtain a minimal value respectively, and all the points on the Pareto front are feasible solutions. Designers can select a preferred point  $C(\zeta_{i_{max}}^*, (l_b + l_e)^*)$  in it according to the trade-off between the precision of kinematic input and the size of whole transmission system. Solving the optimization variable  $\mathbf{x}^*$  in point  $C$ , we can finally get the optimally designed result of the transmission system.

To summarize the design optimization workflows and provide guidance for designers, an optimal design framework of pyramid-shaped transmission system for multi-arm CTR

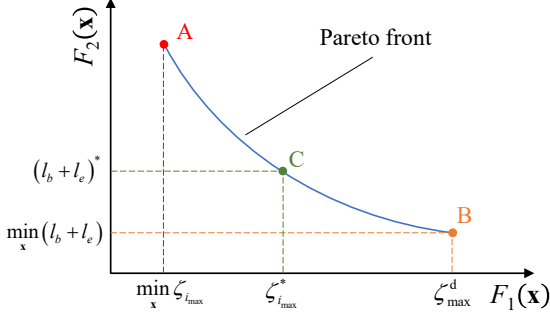


Fig. 8. Schematic diagram of the Pareto front of our multi-objective optimization problem.  $F_1(\mathbf{x})$  is the maximum relative twist angle of each SS tube, and  $F_2(\mathbf{x})$  represents the SS tube length. A and B are the points in which  $F_1(\mathbf{x})$  and  $F_2(\mathbf{x})$  obtain a minimal value, respectively. Point C denotes the optimal values of two objective functions selected by designers.

#### Algorithm 1 Optimal Design Framework of Pyramid-Shaped Transmission System for Multi-Arm CTR.

**Input:**  $a, d, l_c, OD_{N_i}, \Delta L_i, \tau_{i_{max}}, \zeta_{max}^d, (i = 1, 2, \dots, m)$   
**Output:**  $\mathbf{x} = [OD_{S_1}, \dots, OD_{S_m}, l_b, \alpha, l_e, \beta_1, \dots, \beta_{n-1}]^\top$

*Geometric Constraints :*

- 1:  $\mathbf{A} [OD_{S_1}, \dots, OD_{S_m}]^\top \leq \mathbf{b} \leftarrow (7);$
- 2:  $v \leftarrow (12), L_i \leftarrow (13);$
- 3:  $d_j (j = 1, \dots, n) \leftarrow (15)(16)(17);$

*Deformation Constraints :*

- 4:  $\epsilon_{max} \leftarrow (22);$
- 5:  $\zeta_{i_{max}} \leftarrow (27);$

*Optimization :*

- 6: Formulating multi-objective optimization problem (29) which is subject to (30);
- 7: Solving (29)(30), and plotting the Pareto front as Fig. 8;
- 8: Selecting a preferred point C on the Pareto front;
- 9: Getting  $\mathbf{x}^*$  in point C;
- 10: **return**  $\mathbf{x}^*$

is proposed in Algorithm 1. Given the design parameters of NiTi manipulators, we can first establish the geometric and deformation constraints of the transmission system. Then, we sequentially formulate the optimization problem, solve it and get the Pareto front, select a preferred point on the Pareto front, and finally get the optimal  $\mathbf{x}^*$  in the selected point.

#### B. Solving Approach

To solve the optimization problem defined in (29) and (30), the *gamultiobj* command using a controlled, elitist genetic algorithm in MATLAB *Global Optimization Toolbox* is used to create a set of points in the Pareto front.

After selecting the preferred point  $C(\zeta_{i_{max}}^*, (l_b + l_e)^*)$  on the Pareto front, the optimization variable  $\mathbf{x}^*$  can be determined by solving  $\mathbf{x}^* = \arg \min_{\mathbf{x}} F_1(\mathbf{x})$  which is subject to (30) in which  $\zeta_{max}^d = \zeta_{i_{max}}^*$ . Here, the *fmincon* command in MATLAB *Optimization Toolbox* is adopted to get the final  $\mathbf{x}^*$ .

The accompanying code of the proposed framework can be downloaded from [https://github.com/hitzhangchao/CTR/tree/main/Transmission\\_System\\_Optimal\\_Design](https://github.com/hitzhangchao/CTR/tree/main/Transmission_System_Optimal_Design).

TABLE I  
DESIGN PARAMETERS OF THE TWO SETS OF NiTi MANIPULATORS.

Parameters	First Set	Second Set
Number of Arms	$n$	3
Number of Tubes in each Arm	$m$	2
Center Distance between Arms	$a$	5 mm
Straight Sheath Diameter	$d$	12 mm
Straight Sheath Length	$l_c$	80 mm
Outer Diameter (Tube 1)	$OD_{N_1}$	2.70 mm
Inner Diameter (Tube 1)	$ID_{N_1}$	2.40 mm
Radius of Pre-curvature (Tube 1)	$r_1$	135 mm
Curved Length (Tube 1)	$s_1$	160 mm
Translation Distance (Tube 1)	$\Delta L_1$	100 mm
Outer Diameter (Tube 2)	$OD_{N_2}$	2.20 mm
Inner Diameter (Tube 2)	$ID_{N_2}$	1.40 mm
Radius of Pre-curvature (Tube 2)	$r_2$	135 mm
Curved Length (Tube 2)	$s_2$	160 mm
Translation Distance (Tube 2)	$\Delta L_2$	145 mm
Maximum Generated Torque	$\tau_{i_{max}}$	200.0 mNm
Max. Allowable Relative Twist Angle	$\zeta_{max}^d$	8°
	$\zeta_{max}$	5°

#### V. EXPERIMENTS

Based on the optimal design framework, we demonstrate the design of pyramid-shaped transmission systems for two sets of NiTi manipulators whose parameters are tabulated in Table I. Numerical analysis and real-world experiments are conducted to validate the modeling and optimization methods.

#### A. Design Optimization 1 - For the First NiTi Manipulators

The first set of NiTi manipulators is part of a triple-arm CTR, and there are two “SS + NiTi” tubes in each manipulator. So we first define the optimization variable as  $\mathbf{x} = [OD_{S_1}, OD_{S_2}, l_b, \alpha, l_e, \beta_1, \beta_2]^\top$ .

1) *Design Constraints Establishment:* For the geometric constraints, the diameter relations of the “SS + NiTi” tubes are first calculated as  $\mathbf{A} [OD_{S_1}, OD_{S_2}]^\top \leq \mathbf{b}$ , in which  $\mathbf{A} = \begin{bmatrix} 1 & -1 & -1 & 0 \\ 0 & 0 & 1 & -1 \end{bmatrix}^\top$  and  $\mathbf{b} = [5.0, -3.1, -0.4, -2.7]^\top$ . Then, the shape and length of the SS tube are calculated according to (10) and (13), and  $l_{e_{min}}$  is chosen as 40 mm. To avoid collision of the actuation units,  $d_j (j = 1, 2, 3)$  are calculated using (17), and the collision hazard region radius  $r_a$  is chosen as 18 mm.

For the deformation constraints, the SS tubes are made of SUS 316L of which the elastic modulus  $E = 193$  GPa, shear modulus  $G = 72$  GPa, and the tensile yield stress  $\sigma_{0.2} = 310$  MPa. So  $\epsilon_{max}$  should not exceed the elastic strain limit  $\epsilon_e = \sigma_{0.2}/E = 0.16\%$ . Besides, the maximum relative twist angle of SS tubes  $\zeta_{i_{max}}$  is calculated based on (27).

2) *Optimal Design Results:* According to the optimal design framework, we formulate the multi-objective optimization problem as (29), which is subject to constraint (30). Solving the problem using our accompanying code, the Pareto front of the two objective functions can be gotten and is shown in Fig. 9. We can see that the improvement of one objective requires the degradation of another as  $F_1(\mathbf{x})$  increases from 3.36° to 8° while  $F_2(\mathbf{x})$  decreases from 344.8 mm to 291.8 mm.

As all points on the Pareto front are feasible solutions, the variation of the optimization variable  $\mathbf{x}$  with respect to the objective function  $F_1(\mathbf{x})$  has been further characterized as

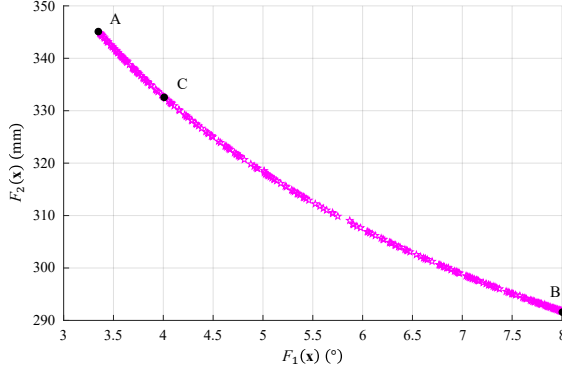


Fig. 9. The Pareto front of the two objective functions.  $F_1(\mathbf{x}) = \zeta_{i_{max}}$  is the maximum allowable relative twist angle of each SS tube, and  $F_2(\mathbf{x}) = l_b + l_e$  represents the SS tube length.

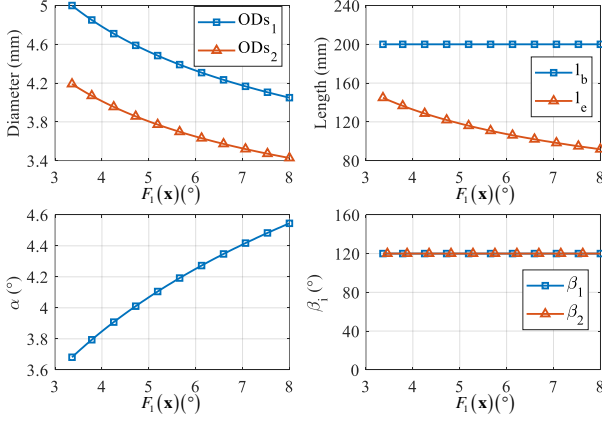


Fig. 10. The variation of optimization variable  $\mathbf{x}$  with respect to the objective function  $F_1(\mathbf{x}) = \zeta_{i_{max}}$ .

shown Fig. 10. As it reveals, if we want a smaller maximum relative twist angle  $\zeta_{i_{max}}$  of SS tube, its diameter  $OD_{s_i}$  needs to be increased and the bending angle  $\alpha$  reduced. The optimization algorithm will increase the SS tube length appropriately, although it is deemed that this will increase  $\zeta_{i_{max}}$ . Besides, the angles  $\beta_1$ ,  $\beta_2$  and  $\beta_3$  between adjacent symmetry planes  $\psi_j$  of each arm are equal as  $120^\circ$ , which indicates these arms should be arranged symmetrically.

After weighing the kinematic input precision and size of the transmission system, we select the point C in Fig. 9 in which  $\zeta_{i_{max}}^* = 4.00^\circ$  and  $(l_e + l_b)^* = 332.8$  mm. The optimally designed results at point A, B and C on the Pareto front as well as an empirically designed result are computed and tabulated in Table II. Meanwhile, these four design results are intuitively plotted in Fig. 11.

3) *Elastic Stability:* As shown in Fig. 12, for the “SS + NiTi” tube pair with optimally and empirically designed SS tubes, their elastic stability has been further considered by plotting the relative rotation angle of the tube pair at the proximal end and the tip. The relative rotation angle of the “SS + NiTi” tube pair is defined as

$$\mu(s) = \theta_2(s) - \theta_1(s), \quad (31)$$

in which  $\theta_2(s)$  and  $\theta_1(s)$  denote rotation angles of the inner and outer “SS + NiTi” tubes at the cross section  $s$ , and  $s$  is

TABLE II  
DESIGN RESULTS OF THE PYRAMID-SHAPED TRANSMISSION SYSTEM  
FOR THE FIRST NiTi TUBE SET

Parameters	Optimal design			Empirical design
	Point A	Point B	Point C	
$OD_{S_1}$	5.00 mm	4.05 mm	4.80 mm	4.00 mm
$OD_{S_2}$	4.19 mm	3.43 mm	4.00 mm	3.00 mm
$l_b$	200.0 mm	200.0 mm	200.0 mm	200.0 mm
$\alpha$	$3.68^\circ$	$4.55^\circ$	$3.85^\circ$	$5.00^\circ$
$l_e$	144.8 mm	91.8 mm	132.8 mm	120 mm
$\beta_1$	$120^\circ$	$120^\circ$	$120^\circ$	$120^\circ$
$\beta_2$	$120^\circ$	$120^\circ$	$120^\circ$	$120^\circ$
$ID_{S_1}$	4.39 mm	3.63 mm	4.20 mm	3.30 mm
$ID_{S_2}$	2.40 mm	2.40 mm	2.40 mm	2.40 mm
$L_1$	524.8 mm	471.8 mm	512.8 mm	500.0 mm
$L_2$	569.8 mm	516.8 mm	557.8 mm	545.0 mm
$\beta_3$	$120^\circ$	$120^\circ$	$120^\circ$	$120^\circ$
$\zeta_{1_{max}}$	$3.36^\circ$	$8.00^\circ$	$4.00^\circ$	$5.91^\circ$
$\zeta_{2_{max}}$	$3.36^\circ$	$8.00^\circ$	$4.00^\circ$	$18.50^\circ$

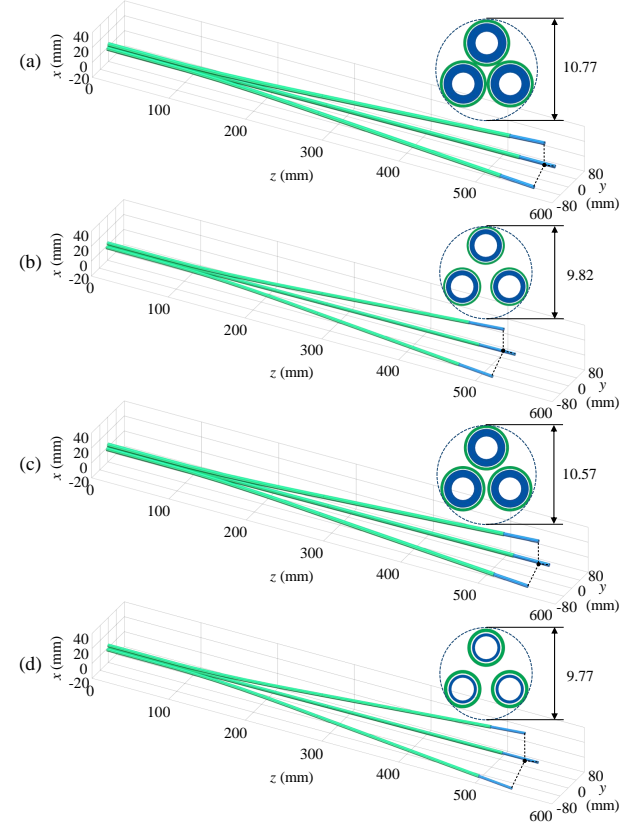


Fig. 11. Design results of SS tubes in the pyramid-shaped transmission system of the triple-arm CTR. (a), (b) and (c) show the optimally designed results referring to the point A, B and C as depicted in Fig. 9, respectively. (d) shows the empirically designed result. The lower left part of each subfigure illustrates the tubes arrangement, and the upper right part illustrates the tube diameters at the output end. The tubes in green and blue represent the outer and inner SS tubes in each arm, respectively.

the arc length starts from the proximal end of the inner tube.

See in Fig. 12, the bottle-green dashed curve is the result with assumption of torsionally rigid SS tubes that will not introduce kinematic errors to the NiTi tubes, which is the ideal situation of the transmission system. The optimally designed SS tubes referring to point A, B and C on the Pareto front bring small kinematic input errors and they all

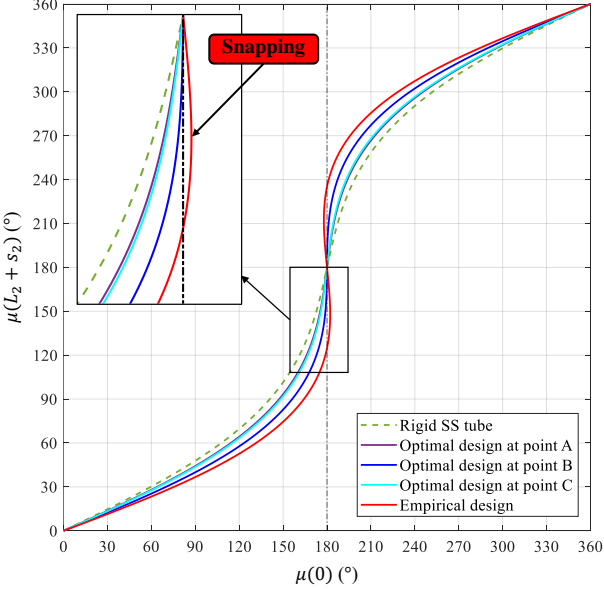


Fig. 12. Relative rotation angle of “SS + NiTi” tube pair at proximal end of SS tubes versus tip of NiTi tubes. Among the four design results in Table II, only the empirically designed one exhibits unstable rotation (snapping).

exhibit stable rotation. In contrast, the empirically designed SS tubes introduce unacceptable kinematic input errors to the NiTi manipulator, which will cause sudden snapping of “SS + NiTi” tubes.

*4) Experiments on Prototype:* As shown in Fig. 13 (a) and (b), two sets of SS tubes were fabricated based on the optimally designed result at point C and the empirically one in Table II. Then, they were bonded to the same set of NiTi tubes successively, and each “SS + NiTi” tube set was assembled as a combined tube pair. A triple-arm CTR prototype with pyramid-shaped transmission system has been constructed as shown in Fig. 13 (d), but only one robotic arm was installed on it for simplicity. Besides, an inclination sensor (WitMotion WT901) with measurement accuracy of  $0.05^\circ$  was mounted at the distal end of the outer SS tube to measure its relative twist angel  $\zeta_1$ . The reason why we choose to measure  $\zeta_1$  is because the maximum relative twist angle  $\zeta_{i\max}$  and tube length  $L_i$  (equivalently represented as  $(l_e + l_b)$ ) of the SS tube are the optimization objectives,  $L_i$  is easily measured, and whether the actual  $\zeta_1$  agrees the theoretical value can be used to evaluate the our modeling and optimization methods.

In the experiments, we first aligned the tube precurvatures of each “SS + NiTi” tube pair. Then, we kept the actuation module of the outer tube stationary while controlling the inner tube to rotate  $1080^\circ$  continuously at a speed of  $6^\circ/\text{s}$ . In this way, the NiTi manipulator changes its curvature because of the elastic interaction between the inner and outer NiTi tubes, which generates the reverse torque  $\tau_i$  to the SS tubes causing the SS tube to undergo the torsional twisting. Meanwhile,  $\zeta_1$  was measured by the inclination sensor at a frequency of 50 Hz. Because of the installation limitations, it is difficult to measure the generated torque and the relative twist angle of an “SS + NiTi” tube at the same time. Therefore, the generated torque applied to the inner SS tube  $\tau_2$  was later measured by a

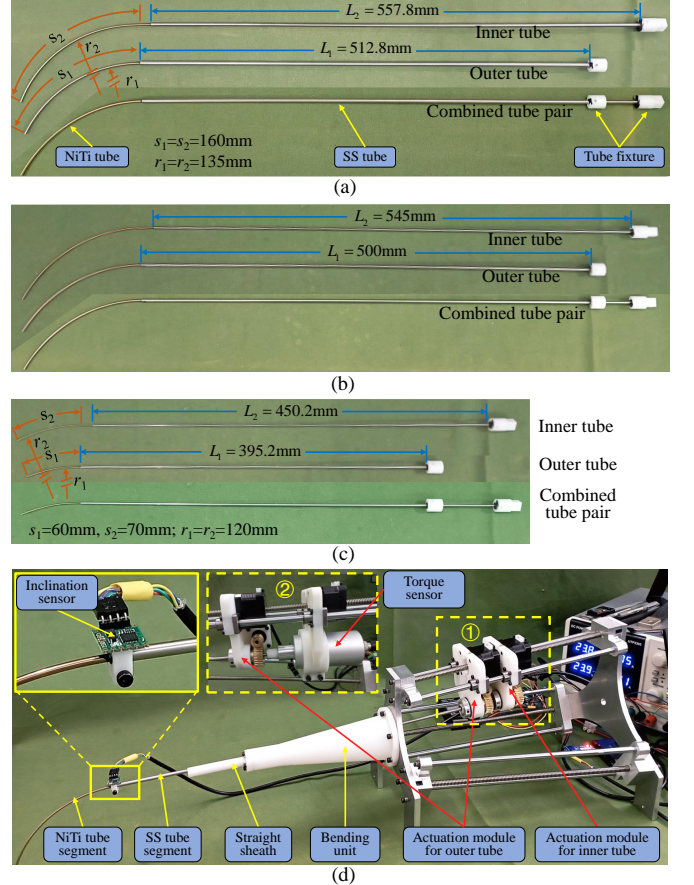


Fig. 13. Robot prototype. (a) shows the fabricated inner and outer “SS + NiTi” tubes with optimally designed parameters at point C in Table II. (b) shows the empirically designed “SS + NiTi” tube pair in Table II. (c) is the optimally designed “SS + NiTi” tube pair in Table III for the second NiTi tube set. (d) illustrates the CTR prototype with pyramid-shaped transmission system. To measure the relative twist angle  $\zeta_1$ , an inclination sensor is attached to the end of outer SS tube. To measure the generated torque  $\tau_i$ , a torque sensor is used by grasping the inner tube’s fixture.

torque sensor (TJGC ATTA05) with measurement accuracy of  $\pm 1.5 \text{ mNm}$  that connected to the inner tube fixture. According to the equilibrium of torsional moments, the torque in outer SS tube  $\tau_1$  equals to  $\tau_2$  with frictional free assumptions.

The measured torque  $\tau_i$  of the tube pair is shown in Fig. 14 (a) and  $\tau_{i\max} = 192.75 \text{ mNm}$ . For the optimally designed SS tubes, the theoretical  $\zeta_1$  can be calculated by substituting the measured  $\tau_i$  into (27), which is shown as the green curve in Fig. 14 (b) and its maximum value  $\zeta_{1\max} = 3.80^\circ$ . Meanwhile, the experimental  $\zeta_1$  directly measured by the inclination sensor is shown as the blue curve and  $\zeta_{1\max} = 4.09^\circ$ . We can see that the experimental values agree well with the calculated ones. As for the empirically designed SS tubes, see the red curve in Fig. 14 (b), severe snapping of the “SS + NiTi” tube pair was observed as the measured  $\zeta_1$  experiences several steep drops, which is consistent with the prediction in Fig. 12.

### B. Design Optimization 2: For the Second NiTi Manipulators

For the second NiTi tube set given in Table I, we need to design a pyramid-shaped transmission system for a four-armed CTR which has two “SS + NiTi” tubes in each arm.

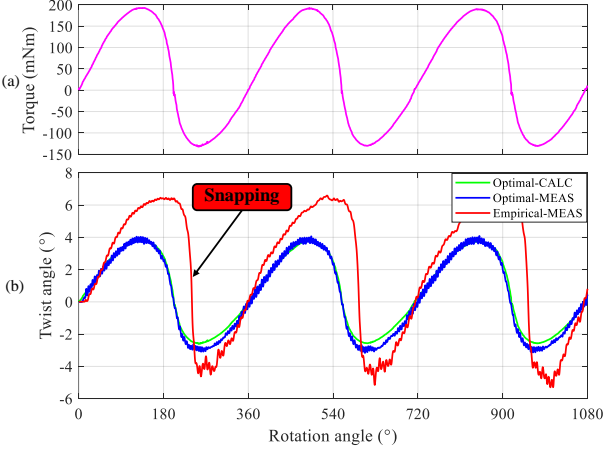


Fig. 14. (a) shows the measured torque  $\tau_i$  of NiTi tube pair versus rotation angle of the outer tube. (b) depicts relative twist angles  $\zeta_1$  of the outer SS tube segment at its distal end. The green and blue lines are the theoretical and experimental values of the optimally designed SS tubes, respectively. The red line is the experimental value of the empirically designed SS tubes, and the tube pair experienced the elastic instability (snapping).

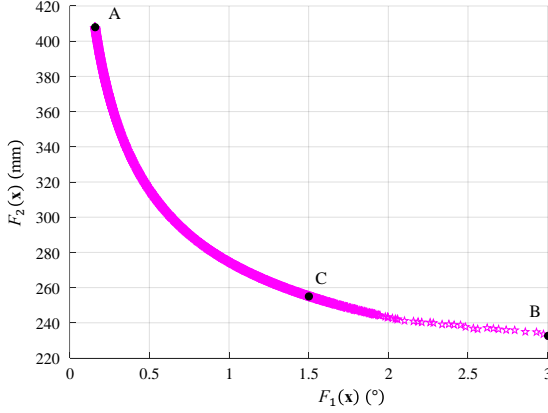


Fig. 15. The Pareto front of the two objective functions  $F_1(\mathbf{x}) = \zeta_{i\max}$  and  $F_2(\mathbf{x}) = l_b + l_e$ .

1) *Optimal Design Results:* According to the proposed optimal design framework, we first define the optimization variable as  $\mathbf{x} = [OD_{S1}, OD_{S2}, l_b, \alpha, l_e, \beta_1, \beta_2, \beta_3]^T$ , then establish the geometric and deformation constraints as done before, and then formulate the optimization problem. Solving the problem, we can get the Pareto front of the two objectives as shown in Fig. 15, and the variation of  $\mathbf{x}$  with respect to  $F_1(\mathbf{x})$  is shown in Fig. 16.

From Fig. 15, when  $F_1(\mathbf{x})$  changes from  $0.17^\circ$  to  $3^\circ$ ,  $F_2(\mathbf{x})$  will be reduced from 407.6 mm to 232.5 mm, that is while  $F_1(\mathbf{x})$  increases by only  $2.83^\circ$ ,  $F_2(\mathbf{x})$  will be significantly shortened by 175.1 mm. It indicates that a small sacrifice in kinematic input accuracy can achieve a large compactness promotion for the transmission system. Therefore, we finally choose the point C on the Pareto front to get a compact system, in which  $\zeta_{i\max}^* = 1.50^\circ$  and  $(l_e + l_b)^* = 255.2$  mm. The optimally designed results at point A, B and C are tabulated in Table III and intuitively plotted in Fig. 17.

2) *Experimental Validation:* According to the optimally designed result in point C for the second NiTi tube set, we

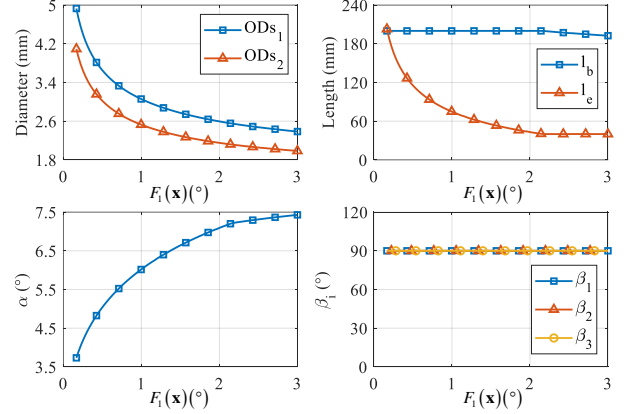


Fig. 16. The variation of optimization variable  $\mathbf{x}$  with respect to the objective function  $F_1(\mathbf{x}) = \zeta_{i\max}$ .

TABLE III  
DESIGN RESULTS OF THE PYRAMID-SHAPED TRANSMISSION SYSTEM  
FOR THE SECOND NiTi TUBE SET

Parameters	Optimal design		
	Point A	Point B	Point C
$OD_{S1}$	4.93 mm	2.39 mm	2.78 mm
$OD_{S2}$	4.10 mm	1.99 mm	2.30 mm
$l_b$	200.0 mm	192.6 mm	200.0 mm
$\alpha$	$5.18^\circ$	$7.43^\circ$	$6.64^\circ$
$l_e$	207.6 mm	40.1 mm	55.2 mm
$\beta_1$	$90^\circ$	$90^\circ$	$90^\circ$
$\beta_2$	$90^\circ$	$90^\circ$	$90^\circ$
$\beta_3$	$90^\circ$	$90^\circ$	$90^\circ$
$ID_{S1}$	4.30 mm	2.19 mm	2.50 mm
$ID_{S2}$	1.46 mm	1.46 mm	1.46 mm
$L_1$	547.6 mm	372.7 mm	395.2 mm
$L_2$	602.6 mm	427.7 mm	450.2 mm
$\beta_4$	$90^\circ$	$90^\circ$	$90^\circ$
$\zeta_{i\max}$	$0.17^\circ$	$3.00^\circ$	$1.50^\circ$
$\zeta_{2\max}$	$0.17^\circ$	$3.00^\circ$	$1.50^\circ$

fabricated an “SS + NiTi” tube pair as shown in Fig. 13 (c) and updated the robot prototype. With the same experimental setup as conducted before, we measured the generated torque  $\tau_i$  and the relative twist angle  $\zeta_1$  to evaluate whether the optimally designed result is consistent with the actual experiment.

The measured torque  $\tau_i$  is shown in Fig. 18 (a) and  $\tau_{i\max} = 9.86$  mNm. As shown in Fig. 18 (b), the green curve is the theoretical  $\zeta_1$  by substituting the measured  $\tau_i$  into (27) and its maximum value  $\zeta_{i\max} = 1.52^\circ$ , the blue curve is the actual  $\zeta_1$  measured by the inclination sensor and  $\zeta_{i\max} = 1.38^\circ$ . In the rising segments of the curves, the calculated and experimentally measured angles agree well; however, in the falling segments, some errors arise between them. The errors mainly originate from the gear backlash of the actuation modules, and also from the clearances and frictions between the inner and outer “SS + NiTi” tubes. In general, the experimental and theoretical  $\zeta_1$  match well, which indicates that the pyramid-shaped transmission system designed based on the proposed framework shows good agreements for the real-world performances.

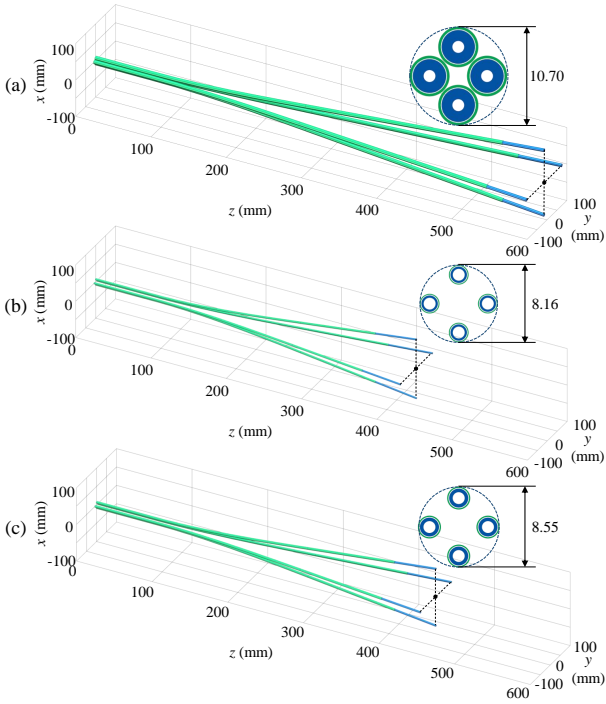


Fig. 17. Design results of SS tubes in the pyramid-shaped transmission system for the four-arm CTR. (a), (b) and (c) show the optimally designed results referring to the point A, B and C as depicted in Fig. 15, respectively.

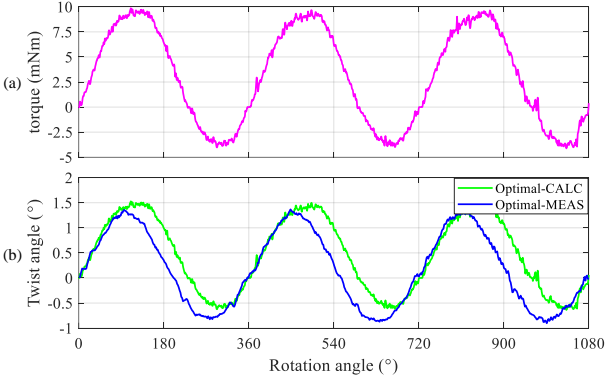


Fig. 18. (a) shows the measured torque  $\tau_2$  of the second NiTi tube pair versus rotation angle of the outer tube. (b) depicts relative twist angles  $\zeta_1$  of the outer SS tube segment at its distal end. The green and blue lines are the calculated and experimental values of the optimally designed SS tubes, respectively.

## VI. CONCLUSIONS

This paper presented an optimal design framework of pyramid-shaped transmission system for multi-arm CTR which uses “NiTi + SS” tubes. Based on our multi-arm CTR, the mechanism of the pyramid-shaped transmission system and the optimization problem behind it were first described. Then, the establishments of the geometric and deformation constraints of the transmission system were introduced. After that, the design problem was formulated as a constrained nonlinear multi-objective optimization problem that minimizes both the twist of tube and the size of whole system. Thorough analyses on the optimal designs by the trade-off between different optimization objectives was presented. According to the proposed framework, the design workflows of the pyramid-

shaped transmission systems for two sets of NiTi manipulators were demonstrated. Finally, numerical analysis and real-world experiments were carried out and validated the efficacy of the proposed modeling and optimization methods. In our future work, an united design optimization framework including the NiTi manipulators and pyramid-shaped transmission system will be investigated based on task and anatomical constraints.

## REFERENCES

- [1] P. E. Dupont, N. Simaan, H. Choset, and C. Rucker, “Continuum robots for medical interventions,” *Proceedings of the IEEE*, vol. 110, no. 7, pp. 847–870, 2022.
- [2] Z. Mitros, S. H. Sadati, R. Henry, L. Da Cruz, and C. Bergeles, “From theoretical work to clinical translation: Progress in concentric tube robots,” *Annual Review of Control, Robotics, and Autonomous Systems*, vol. 5, no. 1, pp. 335–359, 2022.
- [3] J. Burgner-Kahrs, D. C. Rucker, and H. Choset, “Continuum robots for medical applications: A survey,” *IEEE Transactions on Robotics*, vol. 31, no. 6, pp. 1261–1280, 2015.
- [4] N. J. van de Berg, D. J. van Gerwen, J. Dankelman, and J. J. van den Dobbelaer, “Design choices in needle steering—a review,” *IEEE/ASME Transactions on Mechatronics*, vol. 20, no. 5, pp. 2172–2183, 2015.
- [5] P. E. Dupont, J. Lock, B. Itkowitz, and E. Butler, “Design and control of concentric-tube robots,” *IEEE Transactions on Robotics*, vol. 26, no. 2, pp. 209–225, 2010.
- [6] J. Burgner-Kahrs, D. C. Rucker, H. B. Gilbert, P. J. Swaney, P. T. Russell, K. D. Weaver, and R. J. Webster, “A teleoperative system for transnasal surgery,” *IEEE/ASME Transactions on Mechatronics*, vol. 19, no. 3, pp. 996–1006, 2014.
- [7] R. J. Hendrick, S. D. Herrell, and R. J. Webster, “A multi-arm hand-held robotic system for transurethral laser prostate surgery,” in *2014 IEEE International Conference on Robotics and Automation*, 2014, pp. 2850–2855.
- [8] M. F. Rox, D. S. Ropella, R. J. Hendrick, E. Blum, R. P. Naftel, H. C. Bow, S. D. Herrell, K. D. Weaver, L. B. Chambliss, and R. J. Webster III, “Mechatronic design of a two-arm concentric tube robot system for rigid neuroendoscopy,” *IEEE/ASME Transactions on Mechatronics*, vol. 25, no. 3, pp. 1432–1443, 2020.
- [9] H. Yu, L. Wu, K. Wu, and H. Ren, “Development of a multi-channel concentric tube robotic system with active vision for transnasal nasopharyngeal carcinoma procedures,” *IEEE Robotics and Automation Letters*, vol. 1, no. 2, pp. 1172–1178, 2016.
- [10] J. Wang, X. Yang, P. Li, S. Song, L. Liu, and M. Q.-H. Meng, “Design of a multi-arm concentric-tube robot system for transnasal surgery,” *Medical and Biological Engineering and Computing*, vol. 58, no. 3, pp. 497–508, 2020.
- [11] J. D. H. Azimian, T. Looi, “A dual-arm robotic neuroendoscope: Early results,” in *Proc. The Hamlyn Symposium on Medical Robotics*, London, UK, Jun 2016, pp. 34–35.
- [12] Z. Mitros, S. Sadati, C. Seneci, E. Bloch, K. Leibrandt, M. Khadem, L. d. Cruz, and C. Bergeles, “Optic nerve sheath fenestration with a multi-arm continuum robot,” *IEEE Robotics and Automation Letters*, vol. 5, no. 3, pp. 4874–4881, 2020.
- [13] T. L. Bruns, A. A. Remirez, M. A. Emerson, R. A. Lathrop, A. W. Mahoney, H. B. Gilbert, C. L. Liu, P. T. Russell, R. F. Labadie, and K. D. Weaver, “A modular, multi-arm concentric tube robot system with application to transnasal surgery for orbital tumors,” *The International Journal of Robotics Research*, vol. 40, no. 2-3, pp. 521–533, 2021.
- [14] Z. Mitros, M. Khadem, C. Seneci, S. Ourselin, L. Da Cruz, and C. Bergeles, “Towards modelling multi-arm robots: Eccentric arrangement of concentric tubes,” in *2018 7th IEEE International Conference on Biomedical Robotics and Biomechatronics (Biorob)*, 2018, pp. 43–48.
- [15] J. Wang, J. Ha, and P. E. Dupont, “Steering a multi-armed robotic sheath using eccentric precurved tubes,” in *2019 International Conference on Robotics and Automation (ICRA)*, 2019, pp. 9834–9840.
- [16] J. Wang, J. Peine, and P. E. Dupont, “Eccentric tube robots as multiarmed steerable sheaths,” *IEEE Transactions on Robotics*, pp. 1–15, 2021.
- [17] L. Wang, F. C. Pedrosa, and R. V. Patel, “Eccentric-tube robot (etr) modeling and validation,” in *2020 8th IEEE RAS/EMBS International Conference for Biomedical Robotics and Biomechatronics (BioRob)*, 2020, pp. 866–871.

- [18] Z. Mitros, S. Sadati, S. Nousias, L. Da Cruz, and C. Bergeles, "Design and quasistatic modelling of hybrid continuum multi-arm robots," in *2022 International Conference on Robotics and Automation (ICRA)*, 2022, pp. 9607–9613.
- [19] G. Fagogenis, M. Mencattelli, Z. Machaidze, B. Rosa, K. Price, F. Wu, V. Weixler, M. Saeed, J. E. Mayer, and P. E. Dupont, "Autonomous robotic intracardiac catheter navigation using haptic vision," *Science robotics*, vol. 4, no. 29, 2019.
- [20] F.-Y. Lin, C. Bergeles, and G.-Z. Yang, "Biometry-based concentric tubes robot for vitreoretinal surgery," in *2015 37th Annual International Conference of the IEEE Engineering in Medicine and Biology Society (EMBC)*, 2015, pp. 5280–5284.
- [21] P. J. Swaney, R. Lathrop, J. Burgner, K. Weaver, H. B. Gilbert, R. J. Webster, and D. B. Comber, "System, method, and apparatus for configuration, design, and operation of an active cannula robot," U.S. Patent 10,548,630, Feb. 2015.
- [22] C. Bergeles, A. H. Gosline, N. V. Vasilyev, P. J. Codd, P. J. del Nido, and P. E. Dupont, "Concentric tube robot design and optimization based on task and anatomical constraints," *IEEE Transactions on Robotics*, vol. 31, no. 1, pp. 67–84, 2015.
- [23] M. T. Chikhaoui, J. Granna, J. Starke, and J. Burgner-Kahrs, "Toward motion coordination control and design optimization for dual-arm concentric tube continuum robots," *IEEE Robotics and Automation Letters*, vol. 3, no. 3, pp. 1793–1800, 2018.
- [24] X. Yang, S. Song, L. Liu, T. Yan, and M. Q.-H. Meng, "Design and optimization of concentric tube robots based on surgical tasks, anatomical constraints and follow-the-leader deployment," *IEEE Access*, vol. 7, pp. 173 612–173 625, 2019.
- [25] A. Bedford and K. M. Liechti, *Deflection of Beams*. Springer Nature Switzerland AG, 2020, pp. 671–681.
- [26] I. Arrayago, E. Real, and L. Gardner, "Description of stress-strain curves for stainless steel alloys," *Materials & Design*, vol. 87, pp. 540–552, 2015.
- [27] R. Xu, A. Asadian, S. F. Atashzar, and R. V. Patel, "Real-time trajectory tracking for externally loaded concentric-tube robots," in *2014 IEEE International Conference on Robotics and Automation (ICRA)*, 2014, pp. 4374–4379.
- [28] R. Xu and R. V. Patel, "A fast torsionally compliant kinematic model of concentric-tube robots," in *2012 Annual International Conference of the IEEE Engineering in Medicine and Biology Society*, 2012, pp. 904–907.



**Chao Zhang** (Student Member, IEEE) received the B.E. degree in mechanical engineering from Harbin Institute of Technology, Harbin, China, in 2016, and the M.E. degree from Harbin Institute of Technology, Shenzhen (HITSZ), China, in 2020. He is currently pursuing the Ph.D. degree with the School of Mechanical Engineering and Automation at HITSZ. His main research interests include design and control of medical and surgical robots.



**Guangdu Cen** (Student Member, IEEE) received the B.E. degree in mechatronic engineering from Guangxi University, Nanning, China, in 2020. He is currently pursuing the M.S. degree with the Harbin Institute of Technology, Shenzhen, China. His main research interests include medical and surgical robotics, robot motion planning.



**Xing Yang** (Student Member, IEEE) received the B.E. degree in mechanical and electronic engineering from the Shandong University of Science and Technology, Qingdao, Shandong, China, in 2012, and the M.E. degree in mechanical and electronic engineering from the North University of China, Taiyuan, China, in 2016. He is currently pursuing the Ph.D. degree in mechanical engineering with the Harbin Institute of Technology at Shenzhen, Shenzhen, China. From June 2014 to May 2016, he was a Joint Student with the Ningbo Institute

of Materials Technology and Engineering, Chinese Academy of Sciences, Ningbo, China, and his research field was mobile robot's location and navigation. His research interests include surgical robotics and continuum robotics.



**Xinhai Xu** (Member, ASME) received B.S. and M.S. degrees from Harbin Institute of Technology, China (with Honors, 2007 and 2009), and Ph.D. degree from The University of Arizona, USA (2014). He is presently associate professor in School of Mechanical Engineering and Automation at Harbin Institute of Technology, Shenzhen, China. His research interests include hydrogen, electrolysis, and fuel cells. He delivered Invited Talks in ASME ES2021, NEFES2020 and 2021. He is named in World's Top 2% Scientists list in 2020 and 2021.



**Max Q.-H. Meng** (Fellow, IEEE) received the Ph.D. degree in electrical and computer engineering from the University of Victoria, Victoria, BC, Canada, in 1992. He is currently a Professor and the Chairperson of the Department of Electronic and Electrical Engineering, Southern University of Science and Technology, Shenzhen, China, on leave from the Department of Electronic Engineering, The Chinese University of Hong Kong (CUHK), Hong Kong, and also with the Shenzhen Research Institute, The Chinese University of Hong Kong at Shenzhen, Shenzhen, China. He has been a Professor of electronic engineering with CUHK since 2002, after being the Director of the Advanced Robotics and Teleoperation (ART) Laboratory and a Professor for ten years with the Department of Electrical and Computer Engineering, University of Alberta, Edmonton, AB, Canada. He has authored over 500 journal and conference papers. His current research interests include robotics, perception and sensing, human–robot interaction, active medical devices, biosensors and sensor networks, and adaptive and intelligent systems. Prof. Meng is an Elected Member of the Administrative Committee of the IEEE Robotics and Automation Society, and a fellow of the Hong Kong Institution of Engineers and the Canadian Academy of Engineering. He was a recipient of the IEEE Millennium Medal. He has served on many editorial boards.



**Shuang Song** (Member, IEEE) received B.S. degree in Computer Sc. & Tech. from North Power Electric University, M.S. degrees in Computer Architecture from Chinese Academy of Sciences, and his Ph.D. degree in Computer Application Tech. from University of Chinese Academy of Sciences, China, in 2007, 2010 and 2013, respectively. Now he is an Associate Professor in Harbin Institute of Technology, Shenzhen, China. His main research interests include magnetic tracking and actuation for Bioengineering applications.



**Jiaole Wang** (Member, IEEE) received the B.E. degree in mechanical engineering from Beijing Information Science and Technology University, Beijing, China, in 2007, the M.E. degree from the Department of Human and Artificial Intelligent Systems, University of Fukui, Fukui, Japan, in 2010, and the Ph.D. degree from the Department of Electronic Engineering, The Chinese University of Hong Kong (CUHK), Hong Kong, in 2016. He was a Research Fellow with the Pediatric Cardiac Bioengineering Laboratory, Department of Cardiovascular Surgery, Boston Children's Hospital and Harvard Medical School, Boston, MA, USA. He is currently an Associate Professor with the School of Mechanical Engineering and Automation, Harbin Institute of Technology, Shenzhen, China. His main research interests include medical and surgical robotics, image-guided surgery, human–robot interaction, and magnetic tracking and actuation for biomedical applications.